J. Ind. Geophys. Union, 27(1) (2023), 28-36

Image processing on meso-scale photographs of brittle shear zones

Poorvi Hebbar[1], Soumyajit Mukherjee[2]*, and Narayan Bose[2]

[1]Department of Computer Science and Engineering, Indian Institute of Technology Bombay, Powai, Mumbai 400 076, Maharashtra, INDIA
[2]Department of Earth Sciences, Indian Institute of Technology Bombay, Powai, Mumbai 400 076, Maharashtra, INDIA
*Corresponding author: smoumyajitm@gmail.com, smukherjee@iitb.ac.in

ABSTRACT

Study of geologic structures and fabrics from different scales of observation is an indispensable first step in structural geology and other branches of geoscience. We process three selected images of brittle shear zones from quartzite, limestone and schist samples using various methods, steps and filters. Such exercises more effectively detect brittle planes when the planes are not too close-spaced and devoid of white fault gouge. Edge detection methods using fuzzy logic seems to be one of the best methods to detect brittle shear planes more distinctly in meso-scale from photographs acquired from ordinary cameras. Notwithstanding, structural geologists' identification and categorization of structures in the field with naked yet *"trained"* eyes **(or** in other scales of observation), continues to be indispensable.

Keywords: Image interpretation, Brittle shear zone, Filters, Geological structures, Structural geology

INTRODUCTION

Correct geologic interpretation of structures documented in field or from other scales of observations (Mukherjee, 2021) has been of paramount importance in structural geology. Field-sketches were done profusely by the field geologists (Genge, 2020) before cameras became handy. Subsequently, with the advent of digital cameras and smart phones (Novakova and Pavlis, 2017), photography and other structural geolo**gic ac**tivities in the field became quite easy. Having a huge space in the electronic device, geologists now take numerous photographs of geological structures. However, after getting back from field, one may note that not all photographs are of good quality, or in a few images, detail structures are required to be presented. In such cases, geological snaps can be required to undertake image processing. However, if the primary image is poor, chances are that image analysis can help to recover features with a limit (Heilbronner and Barrett, 2014). One of the main outcomes of image analysis in structural geology is to enhance the geologic features of key interest (Bjørnerud and Boyer, 1996) taken in an unbiased, reproducible, quantitative and time-saving way (Bons and Jessell, 1996).

In applied structural geological contexts, images have been processed/analyzed for seismic (Misra and Mukherjee, 2018), boreholes (e.g., Cornet, 2013), microstructures (e.g., Mokhles et al., 2019), remote sensing (e.g., Sulaksana and Hamdani, 2014) etc. Matlab programme has recently been developed to study fracture patters (Healy et al., 2017). Image analyses if done carefully, can produce a good number of outcomes (Bjørnerud and Boyer, 1996). Some of these are calculation of object areas, perimeters/lengths, color/grayscale magnitudes, and for lenticular objects, axial lengths, orientations, x-y centers, point-counting, strain analysis, areal estimation and assessment of lattice and grain-shape preferred orientation.

This work, for the first time, applies several standard image processing methods on structural geological images taken on meso-scale. These methods include image segmentation, fuzzy logic image processing, bilateral filtering and comparison amongst various fracture detection filter techniques. We finally compare different methods/ techniques and comment on the practice to get the best possible interpretation of geologic photographs. Specifically speaking, photographs of brittle sheared rocks were analyzed in the present study. The aim was to identify the sigmoidal brittle shear planes correctly, which can lead to correct interpretation of shear sense. The aim is important in structural geology since, incorrect interpretation of shear sense can lead to misleading tectonic models, as reviewed in Dutta and Mukherjee (2019). Figure 1 presents the brittle shear plane terminologies well established in structural geology.

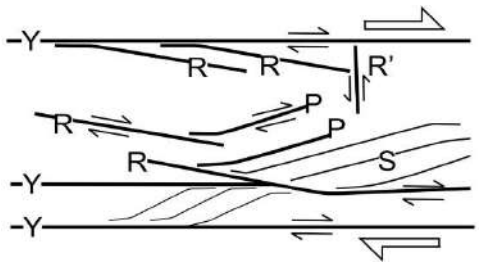

Figure 1. Brittle shear plane nomenclature (reproduced from fig. 5.34 of Passchier and Trouw 1996). P: sigmoid brittle shear plane, S: sigmoid ductile shear plane, R: Riedel brittle secondary shear plane, Y: Primary brittle shear plane.

SCOPE OF WORK

Samples and Photography

Three images (Figures 2a, 3a, 4a) of brittle shear zones with Y- and P-planes developed in different degrees were processed by standard techniques. These photographs were captured using a *Canon PowerShot SX150 IS* digital camera, and they come from the Inner Lesser Himalaya along the Bhagirathi river section (Uttarakhand region of western Himalaya in India). Low-grade meta-sedimentary rocks, mostly quartzites (Fig. 2a) and low-grade metamorphosed limestones (Figures 3a, 4a) and thinly layered schists are present along this traverse. Detail of structural geology of the location can be found in Bose et al. (2018), Bose and Mukherj**ee (2**019), Biswas and Mukherjee (2022) and Biswas et al. (2022). Sigmoid P-planes are bound by Y-planes were found from these images in naked eyes, and in the field a top-to-N/NE back-shear is indicated. The timing of this specific deformation from this Himalayan section has remained unknown till date. Shear zones observed in (sub) vertical natural rock sections were photographed within around 11 a.m. to 02 p.m., i.e. when maximum sun light is available. Rock sections perpendicular to the primary shear Y-planes and parallel to the dip direction of such planes were photographed.

Image processing technique

While interpreting, figures have been named as *"Xyz"* in both main text as well as in the figure captions. Here *X* stands for the methods applied, *y* denotes figure number (*a* for Figure 2a, *b* for Figure 3a and *c* for Figure 4a), and *z* represents steps used in the applied methods (Table 1). For example, *Abc* will mean image segmentation applied on image *b* with RGB to greyscale step involved. Matlab programs were written for each of the image enhancement process (Repository file 1). The image analyses did not have any preferred choice for some specific fractures. For example, the grain boundaries were also enhanced along with the brittle P- and Y-planes. Repository 2 presents all the interpreted images, with about 20 each from the given 3 uninterpreted images. In Discussions section, we present few key images in order to compare the output.

Table 1. Methods and Steps used in different methods.

X in fig. code *Xyz*	Method	*z* in fig. code *Xyz*	Standard approach (Internet ref)
A	Image segmentation	a. Original uninterpreted image	
		b. Contrast stretching	Contrast is augmented in the image: Stretches the intensity range to span a desired range of magnitudes.
		c. RGB to greyscale conversion	Alters RGB Images into gray scale. Average value of the three colors per pixel is taken.
		d. Segmented cracks	Alters the grayscale image into a binary image. Pixels in the input image are altered with a luminance more than a threshold level with the value 1 (white). Other pixels with the magnitude 0 (black).
		e. Cleaned image	Deletes isolated pixels (individual 1's surrounded by 0's or vice-versa).
		f. Thinned image	It removes pixels so that an object without holes shrinks to a minimally connected stroke, and an object with holes shrinks to a connected ring halfway between each hole and the outer boundary.
B	Fuzzy logic image processing	a. Original uninterpreted image	
		b. RGB to greyscale	See *A-c* above
		c. I_x: Gradient of intensities	Gradient of the intensities of image pixels along x-direction.
		d. I_y: Gradient of intensities	Gradient of the intensities of image pixels along y-direction.
		e. Degree of membership	A membership function is assigned with the specified type and parameters. Designates a zero-mean Gaussian membership function for each input. For gradient value for a pixel to be 0, it belongs to the zero membership function with a degree = 1. If sx and sy are the standard deviations for the zero membership function for the Ix and Iy inputs, for edge detector performance, theor

			magnitudes can be altered. Increasing the values renders the algorithm insensitive to the edges and reduces their intensity. Start, peak and end of the triangles of the membership functions can be altered to control the performance of the edge detector.
		f. Edge detection	Ix and Iy values can detect edges and mark as white pixels in the output Image. Pixel is colored white if it comes from a uniform region. It is black otherwise. A pixel is in a uniform region when the image gradient is zero along both the directions. One of these directions with a nonzero gradient means that then the pixel lies on an edge.
C	Bilateral filtering	a. Original uninterpreted image	
		b. RGB to greyscale	See *A-c* above.
		c. Binary gradient mask	Convert the grayscale image into binary image. This is achieved by replacing all pixels in the input image with luminance > a threshold level; value 1 (white) and replacing all other pixels 0 (black).
		d. Dilated gradient mask	Dilate the binary image, i.e., add pixels to the boundaries of objects in an image.
		e. Bilateral filtering	An edge preserving smoothing method, here a mask is made with weights for surrounding pixels and convolve it with the original image. The smoothed intensity at every pixel location x1 = weighted average of the surrounding pixels. The weight for a pixel location x2, for the intensity to be calculated at x1 is: *(i)* spatial distance between x1 and x2 (as the distance increases, weight reduces) *(ii)* dissimilarity between the intensity at x1 and x2 (higher the dissimilarity, reduced is the weight).
D	Comparison between various fracture detection filter techniques	a. Original uninterpreted image	
		b. RGB to greyscale	See *A-c* above
		c. Sobel filter	Uses matrix mathematics to compute areas of different intensities of an image.
		d. Canny filter	Uses a multi-stage algorithm to detect a long range of edges in images.
		e. Prewitt filter	Uses a derivative mask and can detect only horizontal and vertical edges.
		f. Roberts filter	Performs a simple, quick, 2-D spatial gradient measurement. It works on a high spatial frequency region, often corresponding to edges. Matrices used: Gx=[[1 0] [0 -1]], Gy=[[0 1] [-1 0]].
		g. LoG filter	Finds edges by looking for zerocrossings after filtering with a Laplacian of Gaussian (LoG) filter.
		h. Zerocross filter	Finds edges by looking for zero-crossings.
X in fig. code *Xyz*	Method	*z* in fig. code *Xyz*	Standard approach (Internet ref)
A	Image segmentation	g. Original uninterpreted image	
		h. Contrast stretched	Contrast is augmented in the image: Stretches the intensity range to span a desired range of magnitudes.
		i. RGB to greyscale	Alters RGB Images into gray scale. Average value of the three colors per pixel is taken.
		j. Segmented cracks	Alters the grayscale image into a binary image. Pixels in the input image are altered with a luminance more than a threshold level with the value 1 (white). Other pixels with the magnitude 0 (black).
		k. Cleaned image	Deletes isolated pixels (individual 1's surrounded by 0's or vice-versa).
		l. Thinned image	It removes pixels so that an object without holes shrinks to a minimally connected stroke, and an object with holes shrinks to a connected ring halfway between each hole and the outer boundary.

B	Fuzzy logic image processing	g. Original uninterpreted image	
		h. RGB to greyscale	See *A-c* above
		i. I_x: Gradient of intensities	Gradient of the intensities of image pixels along x-direction.
		j. I_y: Gradient of intensities	Gradient of the intensities of image pixels along y-direction.
		k. Degree of membership	A membership function is assigned with the specified type and parameters. Designates a zero-mean Gaussian membership function for each input. For gradient value for a pixel to be 0, it belongs to the zero membership function with a degree = 1. If sx and sy are the standard deviations for the zero membership function for the Ix and Iy inputs, for edge detector performance, theor magnitudes can be altered. Increasing the values renders the algorithm insensitive to the edges and reduces their intensity. Start, peak and end of the triangles of the membership functions can be altered to control the performance of the edge detector.
		l. Edge detection	Ix and Iy values can detect edges and mark as white pixels in the output Image. Pixel is colored white if it comes from a uniform region. It is black otherwise. A pixel is in a uniform region when the image gradient is zero along both the directions. One of these directions with a nonzero gradient means that then the pixel lies on an edge.
C	Bilateral filtering	a. Original uninterpreted image	
		f. RGB to greyscale	See *A-c* above.
		g. Binary gradient mask	Convert the grayscale image into binary image. This is achieved by replacing all pixels in the input image with luminance > a threshold level; value 1 (white) and replacing all other pixels 0 (black).
		h. Dilated gradient mask	Dilate the binary image, i.e., add pixels to the boundaries of objects in an image.
		i. Bilateral filtering	An edge preserving smoothing method, here a mask is made with weights for surrounding pixels and convolve it with the original image. The smoothed intensity at every pixel location x1 = weighted average of the surrounding pixels. The weight for a pixel location x2, for the intensity to be calculated at x1 is: *(i)* spatial distance between x1 and x2 (as the distance increases, weight reduces) *(ii)* dissimilarity between the intensity at x1 and x2 (higher the dissimilarity, reduced is the weight).
D	Comparison between various fracture detection filter techniques	i. Original uninterpreted image	
		j. RGB to greyscale	See *A-c* above
		k. Sobel filter	Uses matrix mathematics to compute areas of different intensities of an image.
		l. Canny filter	Uses a multi-stage algorithm to detect a long range of edges in images.
		m. Prewitt filter	Uses a derivative mask and can detect only horizontal and vertical edges.
		n. Roberts filter	Performs a simple, quick, 2-D spatial gradient measurement. It works on a high spatial frequency region, often corresponding to edges. Matrices used: Gx=[[1 0] [0 -1]], Gy=[[0 1] [-1 0]].
		o. LoG filter	Finds edges by looking for zerocrossings after filtering with a Laplacian of Gaussian (LoG) filter.
		p. Zerocross filter	Finds edges by looking for zero-crossings.

DISCUSSIONS

In the image segmentation method (method *A*), no significant differences are found amongst the uninterpreted image (Figure 2a), the contrast stretched image (Figure 2b), and the greyscale image (Figure 2c). No notable improvement is found also for fuzzy logic image processing (method *B*) when the RGB to greyscale conversion was made (image *Bab* in Repository file 2). However, in case of the segmented crack approach under method *B*, curved P-plane is clearly visible near the middle part of the image (Figure 2d). The cleaned image (Figure 2e) under method *B* shows fractures with equal ease as that of the Figure 2d. When Fuzzy logic image processing (method *B*) with I_X: gradient of intensities is applied, shear zones take an appearance (Figure 2f), which perhaps only a structural geologist who has seen the field exposure (Figure 2a) earlier can interpret. However, when Fuzzy logic image processing (method *B*) with I_y: gradient of intensities is applied, the shear planes are not at all decipherable (image *Bad* in Repository file 2), even though we have a prior idea about the original uninterpreted image (Figure 2a). One of the best manifestations of P and Y-planes appear when edge detection using fuzzy logic is applied (Figure 2g). In this case, the right portion of the image demonstrates both the P and the Y planes quite distinctly. When bilateral filtering (method *C*) is done and different steps applied, there is no significant improvement in identifying the brittle planes Y and P in the obtained images (image *Caa* up to *Cae* in Repository file 2) when compared with the uninterpretd image (Fig. 2a). The LoG (image *Dag* in Repository file 2) and the zero-cross (image *Dah* in Repository file 2) processes yield clumsy output and can be more difficult to identify the planes Y and P, than the simple uninterpreted image (Figure 2a). The Prewitt filter (Figure 2h) and the Roberts filter (Figure 2i) give better and cleaner images.

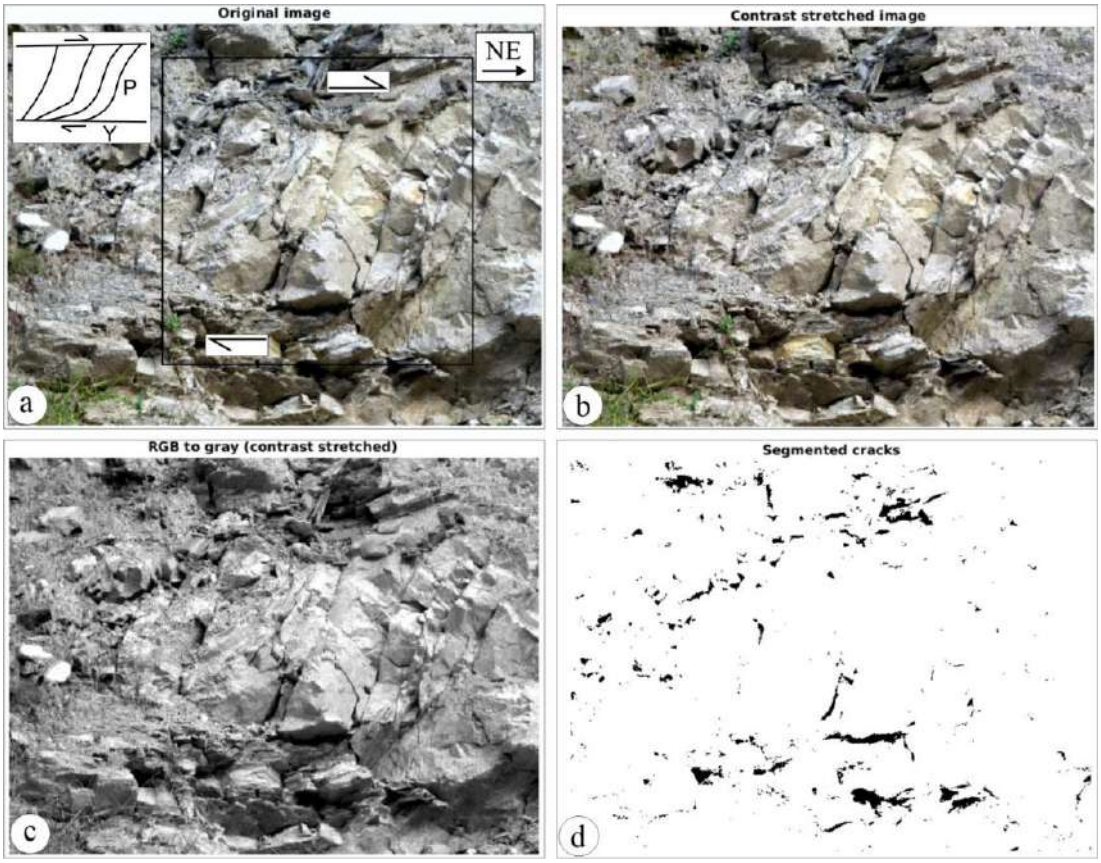

(**Figure 2**, Contd.)

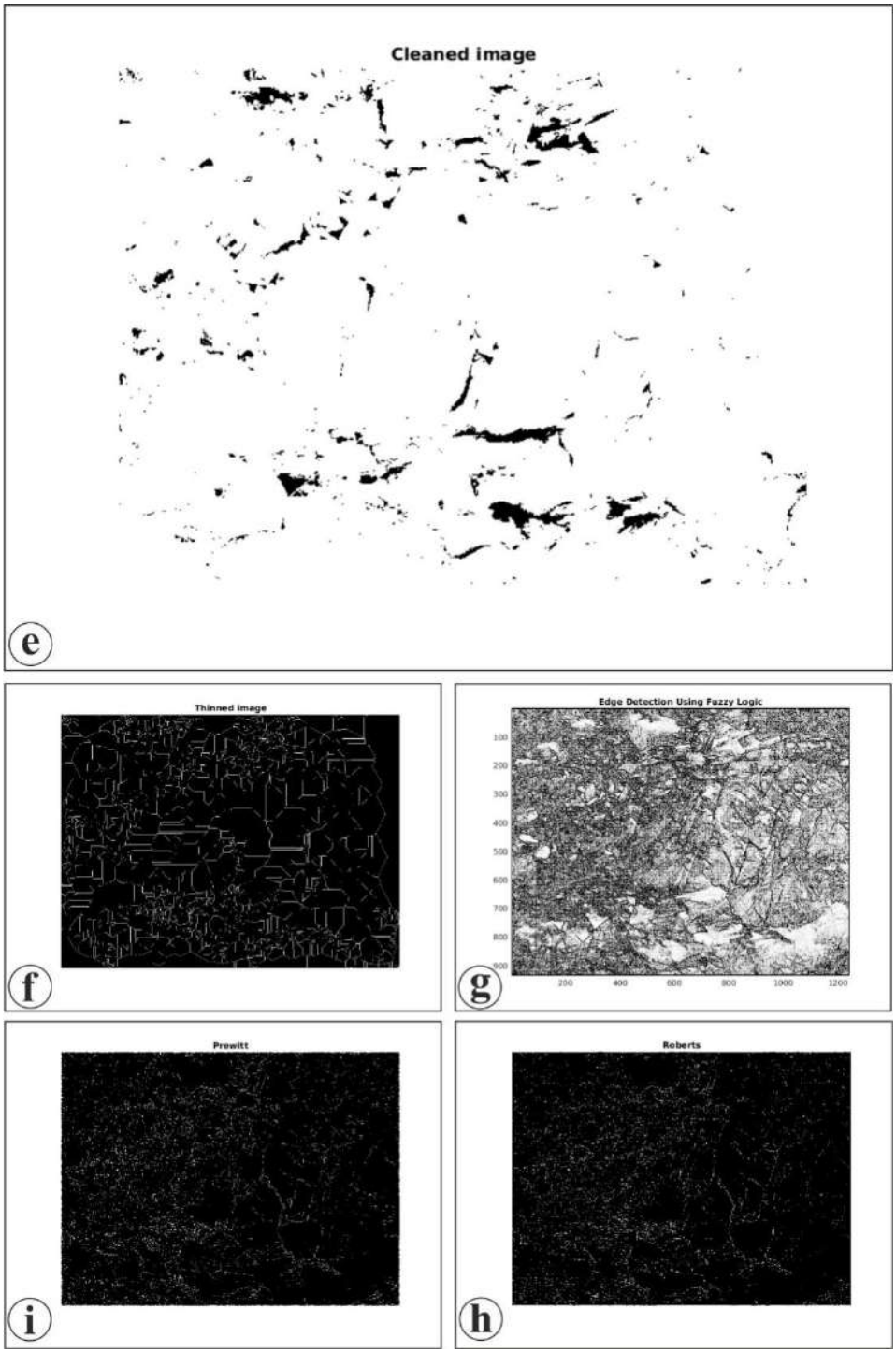

Figure 2. Quartzite exposed at 30.8136°N, 78.6205°E. Width of image ~ 3m. **(a)** *Aaa* (image segmentation to be applied on uninterpreted image 'a'). **(b)** *Aab* (image segmentation applied on image 'a' using contrast stretching method). **(c)** *Aac* (image segmentation applied on image 'a' by RGB to greyscale method). **(d)** *Aad* (image segmentation applied on image 'a' by segmented cracks method). **(e)** *Aae* (image segmentation applied on image 'a' by cleaned image method). **(f)** *Aaf* (image segmentation applied on image 'a' by thinned image method). **(g)** *Baf* (fuzzy logic image processing applied on image 'a' by edge detection method). **(h)** *Dae* (comparison between various fracture detection filter techniques applied on image 'a' using Prewitt filter). **(i)** *Daf* (Comparison between various fracture detection filter techniques applied on image 'a' using Roberts filter). See Table 1 for the codes.

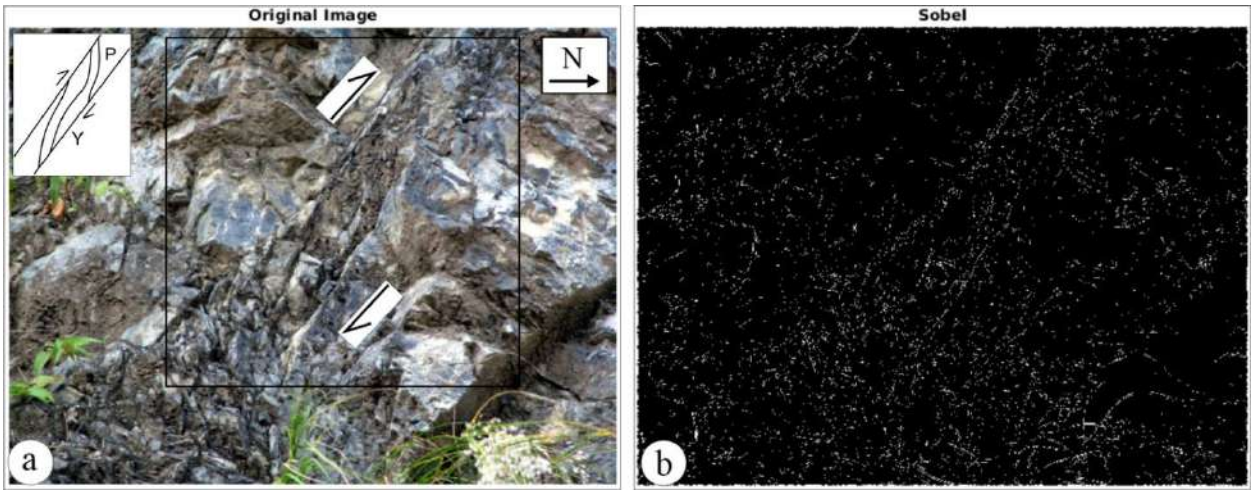

Figure 3. Mandhali Limestone Formati**on ex**posed at 30.6802°N, 78.3497°E. Width of image ~ 3 m. **(a)** *Aba* (image segmentation to be applied on image 'b' on the original uninterpreted image). **(b)** *Dbc (*Comparison between various fracture detection filter techniques applied on image 'b' using the Sobel; filter). See Table 1 for the codes.

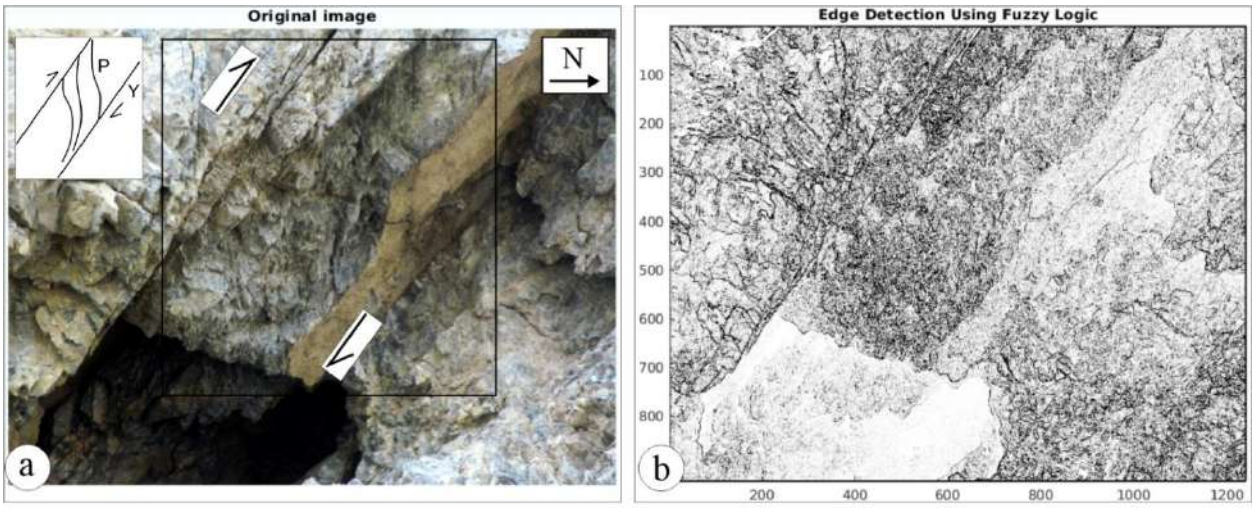

Figure 4. Mandhali Limestone Formation exposed at 30.6802°N, 78.3497°E. Width of image ~ 1.5 m. **(a)** *Aca* (image segmentation to be applied on image 'c' on the original uninterpreted image). **(b)** *Bcf (*Fuzzy logic image processing technique applied on image 'c' by edge detection technioque). See Table 1 for the codes

Interestingly, when we apply image the segmentation method (method *A*) over another uninterpreted image (Figure 3a), segmented crack (image *Abd* in Repository file 2) and cleaned images (image *abe* in Repository file 2) are impossible to decipher for Y and P planes and the shear sense. All the approaches of fuzzy logic image processing (method B) applied on Figure 3a gives unsatisfactory images (images *Bba* to *Bbf* in Repository file 2) that cannot be interpreted for Y and P planes. The same is true for the resultant images (images *Cba* to *Cbe*) in Repository file 2 when bilateral filtering method is applied on Figure 3a. Comparison between various fracture detection filter techniques (method D) when applied on Figure 3a, LoG (image *Dbg* in Repository file 2) and Zerocross filters (image *Dbh* in Repository file 2) give the worst results. The Sobel filter here can produce an image where few of the shear planes are visible (Figure 3b), but still difficult to interpret than the simple visual interpretation of Figure 3a.

In case of the field photograph Figure 4a, following the image segmentation method (method *A*), the segmented crack and the cleaned crack filters give white patches at the place where P- and Y planes are found otherwise. In Fuzzy logic image processing (method *B*), only the edge detection technique

reveals P and Y planes somewhat clearly (Figure 4b). The same problem persists in all the output images (images *Dca* to *Dch* in Repository file 2) in using the method of comparison between various fracture detection filter techniques (method *D*). In bilateral filtering method (method *C*), none of the output images (images *Cca* to *Cce* in Repository file 2) give clear-cut P and Y planes. The different techniques applied for image analyses in this study needs to be cross-checked for other rock types such as gneisses.

The main difference between the two field snaps Figures 2a and 3a is that in the later, the P-planes are more closely spaced than the former one. Possibly because of this, Figure 2a after image processing, gave more distinct appearance of P and Y planes in few cases. Figure 4a is a case with white fault gouge developed where P- and Y planes are found. Because of the white colour, many of the filtering approaches failed to pick up the Y and the P-planes, even though those are visible to the eyes of a trained structural geologist. For all the three starting images Figures 2a, 3a and 4a, their greyscale images deduced by various means do not significantly ease the detection of P and Y planes. In some of the methods, the thinned images and the zero-cross images (e.g., images *Aaf* and *Dch*, respectively in Repository file 2) completely fail to bring out the Y and the P-planes.

CONCLUSIONS

A number of image enhancement methods, techniques and filters are available in public domain. Testing them on meso-scale photographs of brittle shear zones led to following understanding. One of the best manifestations of P and Y-planes appear when edge detection using fuzzy logic is applied.

(i) The zero-cross and the thinned image techniques usually give poor output.

(ii) Greyscale images do not significantly enhance the photographs.

(iii) If the rock consists of white fine-grained contents such as gouge material, image enhancement to detect brittle planes may not work well.

(iv) Image enhancement on close-spaced planes possibly does not ease detection of those planes. For cases *(ii)* to *(iv)*, a trained structural geologist's visual interpretation on field snaps can be more useful! In case, image processing also gives ambiguous results, it will be better to undertake conventional thin-section studies of rocks to detect P and Y-planes in microscale.

Repository Links:

File 1: https://www.geos.iitb.ac.in/wp-content/uploads/2023/01/Repository-file1.pdf

File 2: https://www.geos.iitb.ac.in/wp-content/uploads/2023/01/Repository-file2.pdf

ACKNOWLEDGEMENTS

This work is a part of PH's research assignment for the course *GS 407: Structural Geology* taught by SM. CPDA grant (IIT Bombay) supported SM. Thanks to the Chief Editor Dr. O.P. Pandey and the reviewer Dr. T.R.K. Chetty for providing comments.

Author credit statement

PH: Programming and output images. **SM:** Supervision, manuscript writing, fieldwork. **NB:** Fieldwork, photography, commenting on the draft.

Compliance with Ethical Standards

The authors declare no conflict of interest and adhere to copyright norms.

REFERENCES

Biswas, T. and Mukherjee, S., 2022. Non-Uniform B-spline curve analyses of sigmoid brittle shear P- and ductile shear S-planes. Int. J. Earth Sci., 111, 929–948.

Biswas, T., Bose, N., Dutta, D. and Mukherjee, S., 2022. Arc-parallel shears in collisional orogens: Global review and paleo stress analyses from the NW Lesser Himalayan Sequence (Garhwal region, Uttarakhand, India). Marine Petroleum Geol., 138, 105530.

Bjørnerud, M.G. and Boyer, B., 1996. Image Analysis in Structural Geology Using NIH Image; In: Structural Geology and Personal Computers (ed.) De Paor D, Pergamon Press. Oxford. ISBN: 0 08 042430 9., 105-122.

Bons, P.D. and Jessell, M., 1996. Image Analysis in Structural Geology Using NIH Image; In: Structural Geology and Personal Computers (ed.) De Paor D, Pergamon Press. Oxford. ISBN: 0 08 042430 9, 135-166.

Bose, N. and Mukherjee, S., 2019. Field documentation and genesis of the back-structures from the Garhwal Lesser Himalaya, Uttarakhand, India. In: Sharma, R., Villa, I.M., Kumar, S. (Eds) Crustal Architecture and Evolution of the Himalaya-Karakoram-Tibet Orogen. Geol. Soc., London Spl. Publ., 481, 111–125

Bose, N., Dutta, D. and Mukherjee, S., 2018. Role of grain-size in phyllonitisation: Insights from mineralogy, microstructures, strain analyses and numerical modeling. J. Structural Geol., 112, 39-52.

Cornet, J., 2013. Fracture detection and analysis from image log raw data. Master's thesis. Institutt for petroleumsteknologi og anvendt geofysikk.

Dutta, D. and Mukherjee, S., 2019. Opposite shear senses: Geneses, global occurrences, numerical simulations and a case study from the Indian Western Himalaya. J. Structural Geol., 126, 357-392.

Genge. M.J., 2020. Geological Field Sketches and Illustrations: A Practical Guide. Oxford University Press. ISBN 978–0–19–883592–9., 1-293.

Healy, D. et al., 2017. FracPaQ: A MATLAB™ toolbox for the quantification of fracture patterns. J. Structural Geol., 95, 1-16.

Heilbronner, R. and Barrett, S., 2014. Image Analysis in Earth Sciences: Microstructures and Textures of Earth Materials. Springer-Verlag. Berlin. pp.13. ISBN: 978-3-642-10342-1.

Misra, A.A. and Mukherjee, S., 2018. Seismic Structural Analysis. In: Atlas of Structural Geological Interpretation from Seismic Images. In: Misra, A.A., Mukherjee, S. (Eds.) Wiley Blackwell. ISBN: 978-1-119-15832-5, 15-26.

Mokhles, M., Fatai, A. and Mohammed, M., 2019. Advances in Rock Petrography: Image Processing Techniques for Automated Textural Thin Section Analysis. Society of Petroleum Engineers. SPE-194835-MS.

Mukherjee, S., 2021. Atlas of Structural Geology. Second Edition. Elsevier. Amsterdam. ISBN: 978012816802, 1-260.

Novakova, L. and Pavlis, T.L., 2017. Assessment of the precision of smart phones and tablets for measurement of planar orientations: A case study. J. Structural Geol., 97, 93-103.

Passchier, C.W. and Trouw, R.A.J., 1996. Microtectonics. Springer. pp. 128. ISBN: 978-3-662-08736-7.

Sulaksana, N. and Hamdani, A.M., 2014. The Analysis of Remote Sensing Imagery for Predicting Structural Geology in Berau Basin East Kalimantan. Int. J. Scientific Res., 18-21. Article id: 020131349.

Received on: 24.08.2022; Revised on: 27.12.2022; Accepted on: 15.01.2023